ChemComm

The Efficient Strategy for Improving the Luminescent Sensing Performance of Terbium(III) Metal-Organic Framework Towards Multiple Substances

Journal:	*ChemComm*
Manuscript ID	CC-COM-09-2018-007369.R1
Article Type:	Communication

Journal Name

COMMUNICATION

The Efficient Strategy for Improving the Luminescent Sensing Performance of Terbium(III) Metal-Organic Framework Towards Multiple Substances

Received 00th January 20xx,
Accepted 00th January 20xx

DOI: 10.1039/x0xx00000x

www.rsc.org/

Xiaoning Wang,[1] Jia-Luo Li,[2] Chenggang Jiang,[1] Peng Hu,[1] Bao Li,*[,1] Tianle Zhang[1] and Hong-Cai Zhou*[,2,3]

Abstract: By anchoring triazole units onto the skeleton, the luminescent sensing properties of terbium(III) Metal-Organic Framework could be efficiently improved, including not only expanded the scale of analytes as Fe^{3+}, anions and nitroaromatic molecules, but also enhanced the selectivity and sensitivity.

Lanthanide Metal-Organic Frameworks (Ln-MOFs) have successfully attracted enormous attention owing to their unique advantages and significant luminescence characteristics.[1] With the consideration of potential applications of Ln-MOFs, how to effectively improve the corresponding performances of materials is still a great challenge, since the controllable synthesis of MOFs had not yet come true.[2] Due to the diversity and tunability of MOFs, it had been found that the added function sites decorated onto the final frameworks via the careful pre-design or post-modification would be beneficial for increasing the interactions between host matrix and guest substance that is vital to affect the sensing performance.[3] Therefore, part of attention has been shift towards the exploration of Ln-MOFs-based sensors with high sensitivity and selectivity via introducing the specific functional groups.

Most of the Ln-MOF sensors usually focused on the specific substances, and the examples aimed to detect the different systems or multiple substances with efficient performance is very limited. For example, the Ln-MOFs-based sensors could simultaneously probe Fe^{3+}, $Cr_2O_7^{2-}$, CrO_4^{2-}, and MnO_4^- ions are remarkably rare, and mostly concentrate on the systems of non-aqueous solvents.[4] So it remains a great challenge to exploit Ln-MOFs for detecting these ions in aqueous-phase, particularly for the mixture of pollutant ions. In the light of harmfulness of nitro-aromatic compounds (NACs), developing highly efficient sensors for NACs with fast response time and high sensitivity in both liquid and vapor phase is still a hard task in a long time.[5]

To probe the excellent Ln-MOFs-based sensors for the simultaneous detection of the above ions and NACs, if the additional interaction sites as azoles could be decorated onto the surface or skeleton of MOFs, the luminescent behaviours would be effectively improved.[6] The introduction of azoles will be free with Ln ions and reserve in the final framework, which could not only improve the whole hydrolytic stability of final materials, but also increase the interacting forces via the uncoordinated sites. To elucidate the effect of the strategy, herein, a novel luminescent Tb-MOF, $[Tb_4(L)_6(H_2O)_8]$ (H_2L = 4-{bis(4-benzoic)amino}-4H-1,2,4-triazole, **1**), was successfully constructed, which exhibits multi-responsive behaviors towards Fe^{3+}, $Cr_2O_7^{2-}$, CrO_4^{2-}, MnO_4^- ions and nitromethane, whilst could detect trace amounts of NACs with rapid response in both liquid and vapor phase.

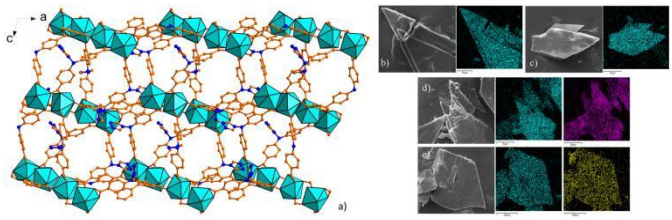

Fig. 1 (a) Partial view of crystal packing mode of **1** showing the irregular porous structures; (b) SEM image of the as-prepared Tb-MOF and EDX mapping image of Tb element; SEM image and EDX mapping image of Tb-MOF after immersed in water for 2 days along with Tb element(c) , in Fe^{3+} solution for half days along with Tb and Fe elements (d), in Co^{2+} solution for half days along with Tb and Co elements (e).

Single-crystal X-ray diffraction analysis indicates that **1** crystallizes in the monoclinic $P2_1/c$ space group (see Table S1†). The asymmetric unit of **1** contains four Tb^{3+} ion, six L^{2-}, and eight coordinated water molecules. Two carboxylate groups of the L^{2-} ligand adopt *syn-syn* and chelating mode to bridge three Tb ions, while the triazole group is free (Figure

[a] *Key laboratory of Material Chemistry for Energy Conversion and Storage, School of Chemistry and Chemical Engineering, Huazhong University of Science and Technology, Wuhan, Hubei, 430074, PR China. E-mail: libao@hust.edu.cn.*
[b] *Department of Chemistry, Department of Materials Science and Engineering, Texas A&M Energy Institute, Texas A&M University,College Station, Texas 77843-3255, United States. E-mail: zhou@chem.tamu.edu*

† Footnotes relating to the title and/or authors should appear here.
Electronic Supplementary Information (ESI) available: Additional experimental sections, characterization and physical measurements (PDF). X-ray crystallographic data for **1** (CIF). CCDC 1843753. For ESI and crystallographic data in CIF or other electronic format see DOI: 10.1039/x0xx00000x

S1†). The four Tb ions in asymmetric unit are inter-connected by two *syn-syn* carboxyl groups to form the linear Tb_4 secondary building unit. All of Tb(III) ions are coordinated by eight oxygen atoms, which can be well described as a distorted triangular dodecahedron geometry (Figure 1). The Tb–O bond distances are in the range of 2.253(6) to 2.506(5) Å, which are comparable to the reported values for other Tb(III)-MOFs.[7] The two terminal and middle Tb ions are coordinated by four and five carboxylate groups, respectively. The remanent sites of Tb ion are occupied by two water molecules (Figure S2a†). Each Tb_4 core is further surrounded by twelve L^{2-} ligands, which is further expanded by another four cores to form the 2D framework (Figure S2b†). All of the Tb_4 cores exhibit two arrangement directions with the twist angle around 72°, which leads to the reservation of irregular porosities in the packing structure (Figure 1), and *sql* network with the Schläfli symbol $\{4^4{\cdot}6^2\}$ calculated with *TOPOS* program. The surface of porous structure is decorated with nitrogen-rich triazole, which must be very useful to capture the guest molecules. The solvent accessible volume in **1** had been calculated as 42.5% by the *PLATON* routine.

The thermal and water stability of title MOF had been investigated via TGA (Figure S5†) and PXRD measurements for different samples immersed in aqueous solution (Figure S3†). The introduction of triazole groups into the final framework and highly-connection mode must be responsible for the intact crystallinity in water solutions containing diverse analytes. The characteristics of porous structure and remnant coordination sites in **1** ensure the even distribution of metallic ions in the composite materials (Figure 1), which could provide a charming platform to achieve the diverse substrates detection.

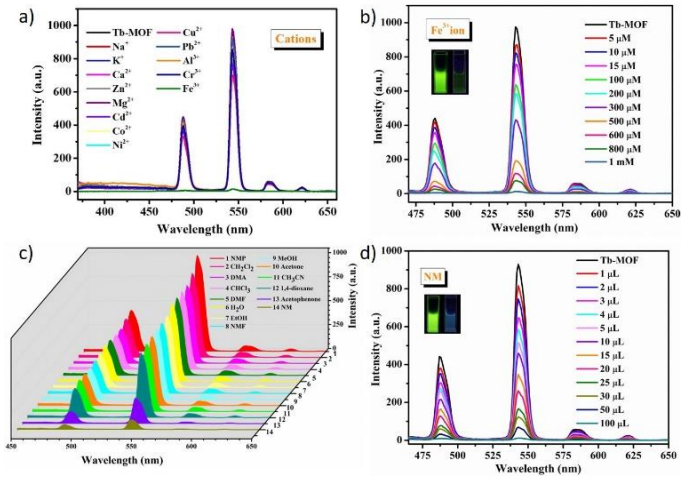

Fig. 2 (a) Luminescence emission spectra of $^5D_4$-$^7F_5$ transitions of **1** immersed into aqueous solution of various cations. (b) Luminescence emission spectra in aqueous solutions containing different concentrations of Fe^{3+} ion. (c) Luminescence emission spectra of $^5D_4$-$^7F_5$ transitions of **1** immersed into aqueous solution of various solvents. (d) Luminescence emission spectra in aqueous solutions with increasing additions of NM.

Different to the free ligand, the solid state of **1** shows characteristic emission peaks of Tb^{3+} ion at 488 nm, 543 nm, 585 nm and 620 nm excited at 365 nm (Figure S6b and S6c†) at room temperature, which could be attributed to the $^5D_4 \rightarrow {}^7F_J$ (J = 6, 5, 4, 3) transitions of the Tb^{3+} ion, respectively, along with the prominent emission of $^5D_4 \rightarrow {}^7F_5$ transition at 543 nm.[8]

Considering the excellent green luminescence properties of **1**, we explore its potential to detect metal cations in water. The grinding samples of **1** were dispersed in aqueous solution (2 mL) containing 10^{-3} M $M(NO_3)_x$. The luminescent spectra related to various metal cations present vividly different effects onto the luminescence of **1** (Figure 2a and Figure S8†), especially for Fe^{3+} ion, which displays a prominent quenching effect with the efficiency of 100%. The competition experiments indicates that **1** exhibits the high selectivity to Fe^{3+} even with the interference of other cations (Figure S9†). A train of luminescence titration experiments also indicate the decrease of luminescence intensity is associated with the concentration of Fe^{3+}. The quenching efficiency which is calculated via the S–V equation evinces that the existence of nearly linear correlation (R^2 = 0.9840) between the quenching efficiency and the quantity of Fe^{3+} at low concentrations (0–100 μM), and the K_{SV} value is estimated to be 1.88 × 10^4 M^{-1} (Figure S10†), which is comparable to those of previously reported Ln-MOFs (Table S4†) and indicates clearly a high sensitivity of **1** for sensing Fe^{3+}.[9] The result indicates that **1** can act as the promising chemical sensors for Fe^{3+} ion.[10] The mechanism of luminescence quenching caused by Fe^{3+} might result from the interactions between cations and the framework or central metals.[10] In X-ray photoelectron spectroscopy (XPS) of solid samples from aqueous solution of Fe^{3+}(Figure S35†), the N 1s peaks at 399.62 eV and 401.32 eV in **1** is shifted to 400.03 eV and 401.70 eV, indicating the weak binding between triazolyl nitrogen atoms and Fe^{3+}.[11] The interaction of weak bonds between the triazolyl nitrogen atoms and Fe^{3+} ions could alert the electronic energy levels of H_2L ligand, further forbid the energy transfer between H_2L ligand and Tb^{3+}, and finally lead to the luminescent quenching.

Simultaneously, the different anions were also selected to carry out the anion-sensing properties of **1** by immersing ground sample in the aqueous solutions of KX with the same concentration (10^{-2} M) (Figure S11a, 11b). $Cr_2O_7^{2-}$, $CrO_4^{2-}$and MnO_4^- give marked luminescence quenching effects, while the other anions have only slight influences on the luminescence intensities. Moreover, the competition experiments have been performed to ascertain the high sensing ability towards $Cr_2O_7^{2-}$, CrO_4^{2-} and MnO_4^- anions. The competition experiments indicates that **1** exhibits the high selectivity to $Cr_2O_7^{2-}$, CrO_4^{2-} and MnO_4^- anions even with the interference of other anions (Figure S11c-11e†). The sensitivity of **1** towards $Cr_2O_7^{2-}$, CrO_4^{2-} and MnO_4^- is examined via concentration-dependent experiments. When the contents of $Cr_2O_7^{2-}$, CrO_4^{2-} and MnO_4^- anions are 2 mM, 2 mM and 500 μM respectively, the luminescence of **1** is almost quenched (Figure S12a-12c†). The quenching constant (K_{SV}) for $Cr_2O_7^{2-}$, CrO_4^{2-} and MnO_4^- were calculated to about 4.1 × 10^3 M^{-1}, 3.9 × 10^3 M^{-1} and 5.18 × 10^4 M^{-1} according to the corresponding S–V plots (Figure S13a-13c†), which are also comparable to those for other reported MOF-based sensors with excellent performance.[12] According to the UV-Vis absorption spectra (Figure S33†), the adsorption spectral of $Cr_2O_7^{2-}$, CrO_4^{2-} and MnO_4^- in aqueous

solution overlap with the excitation peaks of **1**, suggesting that the completion of excitation wavelength energy, which prohibit the energy transfer of efficiency from the ligand to the lanthanide ions, and ultimately results in the luminescence quenching.[4]

Comparably, various organic solvents display markedly different effects onto the luminescence intensity of **1**, especially for nitromethane (NM), which causes an obvious quenching effect (Figure 2c and Figure S14†). To validate the sensitivity towards NM, the fluorescence responses of **1** in the presence of varying quantities of NM had been measured (Figure 2d), the luminescence intensity of **1** was distinctly quenched with the gradually increasing concentration of NM and almost fully quenched after the addition of 100 μL NM with quenching efficiency of 98.75%. The S-V plots for NM exhibited a good linear correlation at low concentrations (Figure S15†) and the calculated K_{SV} values is estimated to be 1.69×10^{-4} M^{-1}, indicating a strong quenching ability of **1** towards NM. The remarkable selectivity of **1** for NM detection could be also validated via the completion experiments of NM with other organic solvents (Figure S16†).

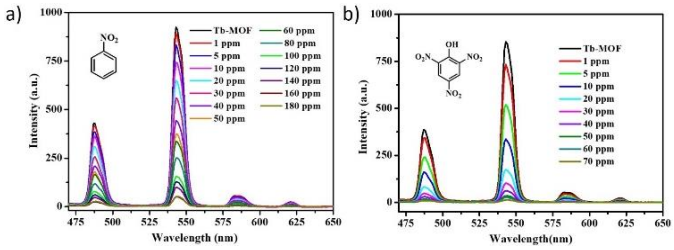

Fig. 3 Fluorescence titration of **1** dispersed in aqueous solution by gradual addition of NB (a) and TNP (b).

The sensing behaviours of **1** to other NACs as nitrobenzene (NB), 1,4-dinitrobenzene(1,4-DNB), 2-nitrotoluene (2-NT), 2,4-dinitrotoluene (2,4-DNT), 1,3-dinitrotoluene (1,3-DNB), and 2,4,6-trinitrophenol (TNP) in aqua solution, had been also investigated (Figure 3a, 3b and Figure S17a-d†). Notably, with the addition of 70 ppm of TNP, the emission could be quenched by 98.5%. The high selectivity of **1** to TNP was further validated by anti-interference studies (Figure S18†). The quenching efficiency could be also quantitatively calculated (Figure S21†), and K_{SV} value is estimated to be 1.51×10^{-1} ppm^{-1}, indicating the high sensitivity of **1** to TNP. Therefore, **1** exhibits the high selectivity and sensitivity towards to TNP in aqueous solution. TNP molecules in aqueous solution tend to be strongly adsorbed by the title Ln-MOF via hydrogen bonding interaction between hydroxyl of TNP and nitrogen atom of triazole, and then the aggregation of TNP molecules would obviously affect the final luminescent properties of composites.

To further monitor trace NACs in the vapor state, the time-dependent fluorescence spectra of **1**-coated thin films placing above the equivalent amount of different NACs in their natural state was monitored. The time-dependent emission spectrums show the different luminescence responses to the vaporized analytes, especially for NB and 2-NT (94% and 85%). The diffusion-controlled process must be responsible for interpreting the identically fast and remarkable fluorescence quenching response for NB and 2-NT (Figure 4). The fluorescence intensity of **1** exposed to NB and 2-NT was on the decline, with a fall of at least 40% within 30 s and 60 s, which reached almost the maxima quenching percentage of 94% and 85% at the time of 600 s. The emission intensity of **1** seemed to approach a fixed level and did not show further changing within a sufficient exposure time. The order of ranking of quenching efficiency is NB＞2-NT＞TNP＞1,3-DNB＞1,4-DNB, which is not fully in accord with the trend of electron deficiency of these NACs. The distinction should refer to the different vapor pressure of analytes (Table S3†).[11] The liquid of NB and 2-NT possess high vapor pressure as well as high electron-withdrawing ability, which contributes to the strongest quenching effect. 2,4-DNT has no impact on the fluorescence intensity of **1** most likely owe to the existence of the electron-donating -CH_3 group in spite of comparable vapor pressure with 1,3-DNB and 1,4-DNB. In addition, the reversible performance of the film against NB vapor was studied. After quenching, the luminescence intensity of **1** can be easily recovered by washing the sample with ethanol several times. Significantly, the fluorescence intensity of the film only has slight decline compared with the initial fluorescence emission after five cycles, meaning good regeneration ability of the film sensors (Figure S31†).

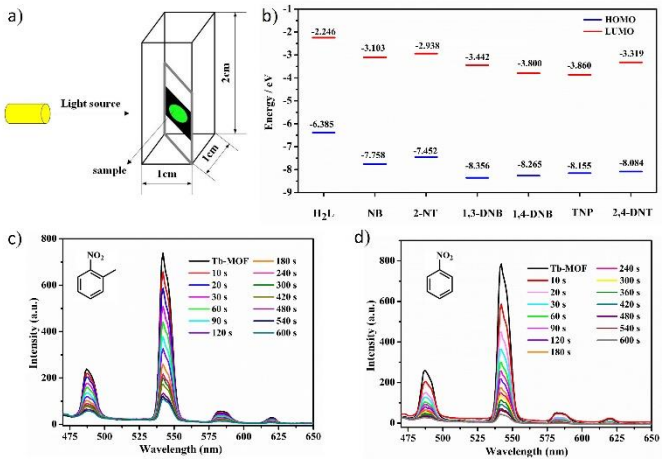

Fig. 4 (a) The home-made setup for the NACs vapor detection. (b) The calculated energy levels for the H_2L ligand and the selected NACs. Time-dependent emission spectrum of **1** in NB vapour (c) and 2-NT vapour (d).

In addition, the mechanism of luminescent quenching behavior for TNP was discussed in detail, which could be of the model for other NACs. TNP has the wide absorption peak and e (molar extinction efficient) in the range at 340−450 nm (Figure S34†), which partially overlaps with the excitation peaks of **1**. Therefore, no matter in aqueous or vapor phase, the energy of the excited light can be strongly absorbed by TNP, which reduces the probability of energy transfer from the H_2L ligand to Tb^{3+}, and ultimately results in the luminescence quenching. On the other hands, the light energy could be also absorbed by the charge transfer from the electron-donating frameworks to the TNP molecules adhered onto the surface of the MOF

particles. The energy of the highest occupied molecular orbit (HOMO) and lowest unoccupied molecular orbit (LUMO) of NACs and the antenna ligand H_2L are calculated by the density functional theory with the level of B3LYP/6-31G**. The H_2L exhibits a high LUMO energy level of −2.2455 eV, higher than the LUMO energy levels of the tested NACs, which facilitates the excited electrons transfer from **1** to the analytes, and then cause the luminescence quenching behaviors. For TNP, it has the lowest LUMO energy level than H_2L and other NACs, and the corresponding charge transfer should be more easily excited. Therefore, once the TNP molecules had been captured onto the surface of **1**, the nature of TNP molecule determines that the luminescent quenching could be attributed to the competition of the absorption of light source energy and the photo-induced electron transfer, which account for the sensitive fluorescent quenching behaviors compared to other NACs.[13]

In summary, guided by the efficient synthesis strategy, a new luminescent Ln-MOF-based sensor with hydrolytic stability has been successfully prepared. The title Tb-MOF is universal to different systems along with the efficient performances, which are prior to or match the parameters of the other Ln-MOFs for the specific substance. The detailed discussions about the sensing mechanism have interpreted the excellent performance of the title Tb-MOF. The corresponding results demonstrate that the quest for new methodologies to assemble luminescent MOFs continues to be of a great impetus, which would contribute to summarize the effective synthesis strategy of sensing materials with high selectivity and sensitivity.

We gratefully acknowledge the National Natural Science Foundation of China (No. 21471062), the Open Project of the State Key Laboratory of Physical Chemistry of the Solid Surface (Xiamen University) (201616), the Center for Gas Separations Relevant to Clean Energy Technologies, an Energy Frontier Research Center (EFRC) funded by the U.S. Department of Energy (DOE), Office of Science, and Office of Basic Energy Sciences (DESC0001015), Office of Fossil Energy, the National Energy Technology Laboratory (DE-FE0026472), and the Robert A. Welch Foundation through a Welch Endowed Chair to HJZ (A-0030) for financial support, and the Analytical and Testing Center, Huazhong University of Science and Technology, for analysis and spectral measurements.

Notes and references

1 (a) Z. C. Hu, B. J. Deibert and J. Li, *Chem. Soc. Rev.,* 2014, **43**, 5815; (b) X. S. Lian, D. Zhao, Y. J. Cui, Y. Yang and G. D. Qian, *Chem. Commun.,* 2015, **51**, 17676; (c) Y. M. Zhang, S. Yuan, G. Day, X. Wang, X. Y. Yang and H.-C. Zhou, *Coord. Chem. Rev.,* 2018, **354**, 28.

2 (a) L. You, D. J. Zha and E. V. Anslyn, *Chem. Rev.*, 2015, **115**, 7840; (b) W. Yan, C. L. Zhang, S. G. Chen, L. J. Han and H. G. Zheng, *ACS. Appl. Mater. Interfaces,* 2017, **9**, 1629; (c) I. Stassen, B. Bueken, H. Reinsch, J. F. M. Oudenhoven, D. Wouters, J. Hajek, V. Van Speybroeck, N. Stock, P. M. Vereecken, R. Van Schaijk, D. De Vos and R. Ameloot, *Chem. Sci.,* 2016, **7**, 5827.

3 (a) D. K. Singha, S. Bhattacharya, P. Majee, S. K. Mondal, M. Kumar and P. Mahata, *J. Mater. Chem. A,* 2014, **2**, 20908; (b) M. H. Zeng, Z. Yin, Z. H. Liu, H. B. Xu, Y. C. Feng, Y. Q. Hu, L. X. Chang, Y. X. Zhang, J. Huang and M. Kurmoo, *Angew. Chem., Int. Ed.,* 2016, **55**, 11407.

4 (a) S. Kumari, C. Panda, S. Mazumdar and S. Sen Gupta, *Chem. Commun.,* 2015, **51**, 15257; (b) T. Jing, L. Chen, F. L. Jiang, Y. Yang, K. Zhou, M. X. Yu, Z. Cao, S. C. Li and M. C. Hong, *Cryst. Growth Des.,* 2018, **18**, 2956; (c) G. P. Li, G. Liu, Y. Z. Li, L. Hou, Y. Y. Wang and Z. H. Zhu, *Inorg. Chem.*, 2016, **55**, 3952.

5 (a) Y. L. Hu, M. L. Ding, X. Q. Liu, L. B. Sun and H. L. Jiang, *Chem. Commun.,* 2016, **52**, 5734; (b) B. Wang, X. L. Lv, D. W. Feng, L. H. Xie, J. Zhang, M. Li, Y. B. Xie, J. R. Li and H.-C. Zhou, *J. Am. Chem. Soc.,* 2016, **138**, 6204; (c) S. S. Nagarkar, B. Joarder, A. K. Chaudhari, S. Mukherjee and S. K. Ghosh, *Angew. Chem., Int. Ed.,* 2013, **52**, 2881.

6 (a) B. Joarder, A. V. Desai, P. Samanta, S. Mukherjee and S. K. Ghosh, *Chem. - Eur. J.,* 2014, **21**, 965; (b) S. S. Nagarkar, A. V. Desai and S. K. Ghosh, *Chem. Commun.,* 2014, **50**, 8915; (c) A. Lan, K. Li, H. H. Wu, D. H. Olson, T. J. Emge, W. Ki, M. C. Hong and J. Li, *Angew. Chem., Int. Ed.,* 2009, **48**, 2334; (d) D. M. Chen, N. N. Zhang, C. S. Liu and M. Du, *J. Mater. Chem. C,* 2017, **5**, 2311.

7 (a) X. G. Liu, H. Wang, B. Chen, Y. Zou, Z. G. Gu, Z. J. Zhao and L. Shen, *Chem. Commun.,* 2015, **51**, 1677; (b) S. Pramanik, Z. C. Hu, X. Zhang, C. Zheng, S. Kelly and J. Li, *Chem. - Eur. J.,* 2013, **19**, 15964; (c) H. M. He, Y. Song, F. X. Sun, Z. Bian, L. X. Gao and G. S. Zhu, *J. Mater. Chem. A,* 2015, **3**, 16598.

8 (a) Y. Yang, F. L. Jiang, L. Chen, J. D. Pang, M. Y. Wu, X. Y. Wan, J. Pan, J. J. Qian and M. C. Hong, *J. Mater. Chem. A,* 2015, **3**, 13526; (b) H. Xu, F. Liu, Y. J. Cui, B. L. Chen and G. D. Qian, *Chem. Commun.,* 2011, **47**, 3153.

9 (a) X. Y. Xu and B. Yan, *ACS Appl. Mater. Interfaces,* 2015, **7**, 721; (b) X. Y. Dong, R. Wang, J. Z. Wang, S. Q. Zang and T. C. W. Mak, *J. Mater. Chem. A,* 2015, **3**, 641; (c) Y. T. Liang, G. P. Yang, B. Liu, Y. T. Yan, Z. P. Xi and Y. Y. Wang, *Dalton Trans.,* 2015, **44**, 13325. (d) S. Dang, E. Ma, Z. M. Sun and H. J. Zhang, *J. Mater. Chem.,* 2012, **22**, 16920. (e) Y. Ning, L. Wang, G. P. Yang, Y. L. Wu, N. N. Bai, W. Y. Zhang and Y. Y. Wang, *Dalton Trans.*, 2016, **45**, 12800.

10 (a) H. Xu, H. C. Hu, C. S. Cao and B. Zhao, *Inorg. Chem.,* 2015, **54**, 4585; (b) G. G. Hou, Y. Liu, Q. K. Liu, J. P. Ma and Y. B. Dong, *Chem. Commun.,* 2011, **47**, 10731; (c) F. L. Hu, Y. X. Shi, H. H. Chen and J. P. Lang, *Dalton Trans.,* 2015, **44**, 18795. (d) Y. L. Wu, G. P. Yang, Y. Q. Zhao, W. P. Wu, B. Liu and Y. Y. Wang, *Dalton Trans.*, 2015, **44**, 3271. (e) Y. L. Wu, G. P. Yang, X. Zhou, J. Li, Y. Ning and Y. Y .Wang, *Dalton Trans.*, 2015, **44**, 10385.

11 (a) B. Liu, W. P. Wu, L. Hou and Y. Y. Wang, *Chem. Commun.,* 2014, **50**, 8733; (b) J. Zhao, Y. N. Wang, W. W. Dong, Y. P. Wu, D. S. Li and Q. C. Zhang, *Inorg. Chem.,* 2016, **55**, 3265; (c) B. L. Chen, L. B. Wang, Y. Q. Xiao, F. R. Fronczek, M. Xue, Y. J. Cui and G. D. Qian, *Angew. Chem., Int. Ed.,* 2009, **48**, 501.

12 (a) S. G. Chen, Z. Z. Shi, L. Qin, H. L. Jia and H. G. Zheng, *Cryst. Growth Des.,* 2017, **17**, 67; (b) Y. N. Lin, X. P. Zhang, W. J. Chen, W. Shi and P. Cheng, *Inorg. Chem.,* 2017, **56**, 11768; (c) W. H. Huang, J. Z. Li, T. Liu, L. S. Gao, M. Jiang, Y. N. Zhang and Y. Y. Wang, *RSC Adv.* 2015, **5**, 97127.

13 (a) J. C. Sanchez and W. C. Trogler, *J. Mater. Chem.,* 2008, **18**, 3143; (b) M. Jurcic, W. J. Peveler, C. N. Savory, D. O. Scanlon, A. J. Kenyon and I. P. Parkin, *J. Mater. Chem. A,* 2015, **3**, 6351. (c) J. H. Qin, B. Ma, X. F. Liu, H. L. Lu, X. Y. Dong, S. Q. Zang and H. W. Hou, *J. Mater. Chem. A,* 2015, **3**, 12690; (d) S. Pramanik, C. Zheng, X. Zhang, T. J. Emge and J. Li, *J. Am. Chem. Soc.,* 2011, **133**, 4153.

